Loss-Aware Optimal Power Sharing in DC Grid-Connected Microgrids for Rural Electrification: An SOCP Approach

Shankar Ramharack
Trinidad and Tobago
sramharack@ieee.org

***Abstract*—This paper presents a loss-aware optimal power flow (OPF) framework for DC community microgrids composed of prosumer nanogrids, targeting rural electrification in energy-poor regions. The framework models both distribution losses in the DC network and power electronic converter losses at each nanogrid, formulated via the branch flow model (BFM) for DC systems. Two formulations are compared: OPF-1, which minimises distribution losses only, and OPF-2, which jointly minimises distribution and converter losses. The resulting non-convex quadratically constrained quadratic program (QCQP) is relaxed to a second-order cone program (SOCP), whose exactness is verified post-solve. A multi-period (24-hour) dispatch with battery state-of-charge coupling is solved across three test cases of increasing complexity: a 7-bus radial system, a modified IEEE 14-bus DC system, and a novel 20-bus clustered-ring topology. Results demonstrate that OPF-2 reveals significant hidden converter losses that OPF-1 entirely neglects, and that the SOCP relaxation is tight across all test cases, confirming global optimality.**

***Index Terms*—Branch flow model, DC microgrids, optimal power flow, SOCP relaxation, peer-to-peer energy sharing, converter losses, rural electrification.**

I. Introduction

Access to reliable electricity remains one of the most pressing challenges for rural communities worldwide. The International Energy Agency (IEA) reports that approximately 770 million people—predominantly in Sub-Saharan Africa and South Asia—still lack access to electricity [1]. Extending national grids to remote areas is prohibitively expensive due to high infrastructure costs, significant transmission losses, and unreliable service with frequent load shedding [2]. Direct current (DC) microgrids powered by solar photovoltaic (PV) panels and battery storage have emerged as a scalable, cost-effective alternative for rural electrification [3], [4].

In a distributed generation distributed storage (DGDS) architecture, each household operates as an independent *nanogrid*—a prosumer unit comprising PV generation, battery storage, and DC loads interconnected via DC-DC converters [5]. Multiple nanogrids are interconnected to form a community microgrid, enabling peer-to-peer power sharing that improves resource utilisation and lowers the levelised cost of electricity (LCOE) compared to isolated solar home systems [3].

The optimal power flow (OPF) problem for such systems seeks to determine the dispatch of generation, storage, and power transfers that minimises total system losses while satisfying network and operational constraints. However, the OPF problem is inherently non-convex due to the quadratic relationship between voltage, current, and power in the network equations, making it NP-hard in general [9].

A. Research Gap and Contributions

Existing literature on DC microgrid OPF predominantly focuses on minimising distribution losses (resistive I^2R losses in the network), while neglecting or oversimplifying power electronic conversion losses [7], [8]. Khan et al. [5], [6] identified this gap and proposed a formulation (OPF-2) that incorporates converter losses alongside distribution losses. However, several open challenges remain:

1) Most studies consider only islanded operation; grid-connected modes with import/export pricing are under-explored for rural DC systems.
2) Clustered topologies with inter-cluster ring connections—common in practical village layouts—have not been systematically studied.
3) The impact of converter loss modelling fidelity on dispatch decisions and the number of active converters has not been quantified across multiple test cases of varying scale.

This paper makes the following contributions:

1) A rigorous mathematical formulation of the loss-aware OPF for DC microgrids, clearly stating all assumptions and classifying the resulting optimisation problem.
2) An SOCP relaxation with post-solve exactness verification across three test cases.
3) A 24-hour multi-period dispatch framework with battery state-of-charge (SOC) coupling.
4) A novel 20-bus clustered-ring test case representative of practical village microgrid layouts.
5) A systematic comparison of OPF-1 (distribution losses only) versus OPF-2 (distribution + converter losses)

demonstrating the significance of converter loss modelling.

II. Literature Review

A. DC Microgrid Architectures for Rural Electrification

DC microgrids for rural electrification can be classified by their generation and storage architecture: centralised generation centralised storage (CGCS), centralised generation distributed storage (CGDS), distributed generation centralised storage (DGCS), and distributed generation distributed storage (DGDS) [5]. DGDS systems offer superior scalability, modularity, and efficiency and are the focus of this work. Nasir et al. [3] proposed scalable DC microgrid architectures and demonstrated the viability of PV-battery-based nanogrids. Madduri et al. [2] presented a practical DGDS implementation for emerging regions.

B. Power Sharing and Dispatch Strategies

Power sharing in DC microgrids is achieved through three main paradigms: (i) droop-based decentralised control, which is simple but suboptimal [10]; (ii) centralised economic dispatch, which yields globally optimal solutions but requires full communication infrastructure; and (iii) distributed optimisation (e.g., ADMM), which balances optimality with communication requirements [4]. This paper adopts the centralised approach, as it establishes the performance benchmark against which distributed methods are measured.

C. Optimal Power Flow in DC Networks

Gan and Low [7] established that the OPF for DC networks can be formulated as a QCQP via the branch flow model (BFM), and that SOCP relaxation is exact under mild conditions for radial networks. Li et al. [8] extended this to stand-alone DC microgrids with PV and storage. Khan et al. [5] further enhanced the BFM to incorporate converter losses, demonstrating that neglecting converter losses leads to suboptimal dispatch decisions on a modified IEEE 14-bus system.

D. Converter Loss Modelling

Kolar et al. [11] and Gelani et al. [12] demonstrated that DC-DC converter efficiency is a non-linear function of loading ratio, not a constant. Khan et al. [5] modelled converter efficiency as a second-order polynomial $\eta_c = k_0 + k_1(P_o/P_R) + k_2(P_o/P_R)^2$, which captures constant, linear, and quadratic loss components. This is the model adopted in this work.

III. System Model

A. Nanogrid Model

Each household in the community is modelled as an independent nanogrid comprising:

- A rooftop solar PV panel with generation P_{G_i} (W).
- A battery with capacity C_B (Wh), state of charge SOC_i (%), and charge/discharge power P_{B_i} (W).
- A DC load with demand P_{L_i} (W).
- A DC-DC converter processing power between the nanogrid and the external bus, with associated conversion losses P_{conv_i} (W).

The nanogrid can function as a *prosumer* (exporting surplus power) or a *consumer* (importing power from neighbours), depending on the instantaneous balance of generation, load, and storage.

B. Network Model: Branch Flow Model for DC Systems

The distribution network is modelled as a connected graph $\mathcal{G}(\mathcal{N}, \mathcal{E})$ where $\mathcal{N} := \{1, 2, \ldots, n\}$ is the set of buses (nanogrid external buses) and $\mathcal{E} \subseteq \mathcal{N} \times \mathcal{N}$ is the set of distribution lines. Each branch $(i, j) \in \mathcal{E}$ has impedance $z_{ij} = r_{ij} + jx_{ij}$. Since the system is DC, the reactance is zero ($x_{ij} = 0$), giving purely resistive impedance $z_{ij} = r_{ij}$.

Variable definitions. For each bus $i \in \mathcal{N}$:

- $v_i := |V_i|^2$ (squared voltage magnitude, V^2)
- P_i (net real power injection, W)

For each branch $(i, j) \in \mathcal{E}$:

- P_{ij} (real power flow from i to j at the sending end, W)
- $l_{ij} := |I_{ij}|^2$ (squared current magnitude, A^2)

Since all quantities are real-valued in a DC system, the BFM is governed by three fundamental relations derived from Ohm's law, Kirchhoff's current law, and the power equation:

$$\text{Ohm's Law:} \quad I_{ij} = g_{ij}(V_i - V_j) \quad \forall (i,j) \in \mathcal{E} \tag{1}$$

$$\text{Current Balance:} \quad I_i = \sum_{j:j\sim i} I_{ij} \quad \forall i \in \mathcal{N} \tag{2}$$

$$\text{Power Equation:} \quad P_i = V_i I_i \quad \forall i \in \mathcal{N} \tag{3}$$

where $g_{ij} = 1/r_{ij}$ is the branch conductance. From these, the BFM equations are derived as:

$$P_{ij} + P_{ji} = r_{ij}\, l_{ij} \quad \forall (i,j) \in \mathcal{E} \tag{4}$$

$$v_i - v_j = r_{ij}(P_{ij} - P_{ji}) \quad \forall i \to j \tag{5}$$

$$v_i \cdot l_{ij} = P_{ij}^2 \quad \forall i \sim j \tag{6}$$

Physical interpretation. Equation (4) states that the total power entering a branch from both ends equals the resistive loss $r_{ij} I_{ij}^2$. Equation (5) relates the squared voltage drop to the net power flow. Equation (6) couples voltage, current, and power—this is the non-convex constraint that makes the OPF problem NP-hard.

C. Distribution Losses

The total distribution loss in the network is:

$$DL = \sum_{(i,j)\in\mathcal{E}} r_{ij}\, l_{ij} = \sum_{(i,j)\in\mathcal{E}} r_{ij} |I_{ij}|^2 \tag{7}$$

D. Converter Loss Model

The efficiency of a DC-DC converter is a non-linear function of its loading ratio $x = P_o/P_R$, where P_o is the output power and P_R is the rated power. Following [5], a second-order polynomial approximation is used:

$$\eta_c(x) = k_0 + k_1\, x + k_2\, x^2 \tag{8}$$

where k_0, k_1, k_2 are empirical coefficients obtained from manufacturer datasheets (typical values: $k_0 = 0.60$, $k_1 = 0.65$, $k_2 = -0.31$, giving peak efficiency $\approx 90\%$ at 60–70% loading). The converter power loss at node i is:

$$P_{\text{conv}_i} = \frac{1-\eta_c}{\eta_c}\, P_o \tag{9}$$

For computational tractability, a direct quadratic loss model is used [6]:

$$P_{\text{conv}_i} = \alpha + \beta\, |P_i^{\text{inj}}| + \gamma\, (P_i^{\text{inj}})^2 \tag{10}$$

where α captures no-load losses, β the linear component, and γ the quadratic component. This is a convex function in $|P_i^{\text{inj}}|$, which preserves tractability.

E. Battery Dynamics

Battery state of charge evolves over time as:

$$SOC_i(t+1) = SOC_i(t) + \frac{1}{C_B} P_{B_i}(t) \quad \forall i \in \mathcal{N} \tag{11}$$

where $P_{B_i} > 0$ denotes charging and $P_{B_i} < 0$ denotes discharging.

F. Assumptions

The following assumptions are made throughout this work:

1) **Steady-state operation:** The system operates in quasi-steady-state at each hourly time step. Transient dynamics (switching, inrush currents) are neglected.
2) **Purely resistive network:** Since the system is DC, line impedance is purely resistive ($x_{ij} = 0$). This is exact for DC systems.
3) **Lossless PV model:** PV generation is modelled as an ideal controllable source bounded by the available irradiance. MPPT losses are absorbed into the converter loss model.
4) **Ideal battery model:** Coulombic efficiency is assumed to be unity. Battery degradation and calendar ageing are not modelled.
5) **Single-port converter:** Each nanogrid has a single DC-DC converter aggregating all internal power flows. The converter loss model uses a quadratic polynomial approximation.
6) **Perfect communication:** The centralised OPF assumes full observability and instantaneous communication between all nanogrids and the central controller.
7) **Balanced loads:** All nanogrids are modelled as single-phase DC systems with deterministic load and generation profiles.
8) **No grid connection in baseline:** The baseline formulation considers islanded operation. Grid-connected extensions are noted as future work.

IV. Optimisation Problem Formulation

A. Sets and Indices

- $\mathcal{N} = \{1, \ldots, n\}$: set of buses (nanogrids).
- $\mathcal{E} \subseteq \mathcal{N} \times \mathcal{N}$: set of distribution branches.
- $\mathcal{T} = \{1, \ldots, T\}$: set of time steps (hours), $T = 24$.
- $\mathcal{C} = \{1, \ldots, C\}$: set of clusters (for TC3).

B. Decision Variables

At each time step $t \in \mathcal{T}$:

- $P_{G_i}(t) \geq 0$: PV generation dispatch at bus i.
- $P_{B_i}(t)$: battery charge (> 0) / discharge (< 0) power.
- $P_{ij}(t)$: power flow on branch (i, j) from i to j.
- $v_i(t) \geq 0$: squared voltage magnitude at bus i.
- $l_{ij}(t) \geq 0$: squared current on branch (i, j).
- $SOC_i(t) \in [0, 1]$: battery state of charge.
- $P_{\text{conv}_i}(t) \geq 0$: converter loss at bus i (OPF-2 only).

C. OPF-1: Distribution Loss Minimisation (Baseline)

$$\textbf{OPF-1:} \quad \min \sum_{t \in \mathcal{T}} \sum_{(i,j) \in \mathcal{E}} r_{ij}\, l_{ij}(t) \tag{12}$$

This is the standard formulation in the literature [7], [8] and serves as the baseline.

D. OPF-2: Joint Distribution and Converter Loss Minimisation

$$\textbf{OPF-2:} \quad \min \sum_{t \in \mathcal{T}} \left[\sum_{(i,j) \in \mathcal{E}} r_{ij}\, l_{ij}(t) + \sum_{i \in \mathcal{N}} P_{\text{conv}_i}(t) \right] \tag{13}$$

This is the proposed formulation that captures total system losses. Both OPF-1 and OPF-2 are subject to the following constraints for all $t \in \mathcal{T}$.

E. Constraints

1) Power Balance at Each Node:

$$P_{G_i}(t) - P_{L_i}(t) - P_{B_i}(t) - P_{\text{conv}_i}(t) = P_i^{\text{inj}}(t) \quad \forall i \in \mathcal{N} \tag{14}$$

where the net injection P_i^{inj} is defined as:

$$P_i^{\text{inj}}(t) = \sum_{j : i \to j} P_{ij}(t) + \sum_{j : j \to i} P_{ji}(t) \quad \forall i \in \mathcal{N} \tag{15}$$

For OPF-1, $P_{\text{conv}_i}(t) = 0$ in (14).

2) Branch Flow Model Constraints:

$$P_{ij}(t) + P_{ji}(t) = r_{ij}\, l_{ij}(t) \qquad \forall (i,j) \in \mathcal{E} \tag{16}$$

$$v_i(t) - v_j(t) = r_{ij}\big(P_{ij}(t) - P_{ji}(t)\big) \qquad \forall i \to j \tag{17}$$

$$v_i(t) \cdot l_{ij}(t) = P_{ij}(t)^2 \qquad \forall i \sim j \tag{18}$$

Equations (16)–(17) are linear. Equation (18) is a non-convex quadratic equality, which makes the overall problem a QCQP.

3) Operational Limits:

$$l_{ij}(t) \le I^2_{ij,\text{rated}} \qquad \forall (i,j) \in \mathcal{E} \tag{19}$$

$$\underline{v}_i \le v_i(t) \le \overline{v}_i \qquad \forall i \in \mathcal{N} \tag{20}$$

$$\underline{P}_{G_i} \le P_{G_i}(t) \le \overline{P}_{G_i}(t) \qquad \forall i \in \mathcal{N} \tag{21}$$

where $\underline{v}_i = (0.95)^2$ p.u. and $\overline{v}_i = (1.05)^2$ p.u. are the squared voltage limits.

4) Battery Constraints:

$$SOC_i(t+1) = SOC_i(t) + \frac{P_{B_i}(t)}{C_B} \qquad \forall i \in \mathcal{N} \tag{22}$$

$$\underline{SOC}_i \le SOC_i(t) \le \overline{SOC}_i \qquad \forall i \in \mathcal{N} \tag{23}$$

5) Converter Loss Constraints (OPF-2 Only):

$$P_{\text{conv}_i}(t) \ge \alpha + \beta\, P_{o_i}(t) + \gamma\, P_{o_i}(t)^2 \tag{24}$$

$$P_{o_i}(t) \ge |P^{\text{inj}}_i(t)| \tag{25}$$

where P_{o_i} is an auxiliary variable representing the absolute power processed by the converter, and (α, β, γ) are the quadratic loss coefficients.

V. SOCP Relaxation and Optimisation Considerations

A. Problem Classification

The OPF problem defined by (13)–(24) is a *quadratically constrained quadratic program* (QCQP) due to:

- The non-convex quadratic equality (18): $v_i \cdot l_{ij} = P^2_{ij}$.
- The quadratic terms in the converter loss model (24): $\gamma P^2_{o_i}$.
- For OPF-1, the objective is linear in l_{ij}, but the constraint (18) remains non-convex.

This QCQP is non-convex and NP-hard in general [9]. A direct solution would require non-linear solvers with no guarantee of global optimality.

B. SOCP Relaxation

The key insight, due to Gan and Low [7], is to *relax* the non-convex equality (18) to a convex inequality:

$$v_i(t) \cdot l_{ij}(t) \ge P_{ij}(t)^2 \quad \forall (i,j) \in \mathcal{E},\ t \in \mathcal{T} \tag{26}$$

This is a *rotated second-order cone* (SOC) constraint, since it can be rewritten as:

$$\left\| \begin{pmatrix} 2P_{ij} \\ v_i - l_{ij} \end{pmatrix} \right\|_2 \le v_i + l_{ij} \tag{27}$$

with $v_i \ge 0$ and $l_{ij} \ge 0$.

With this relaxation, all remaining constraints are linear or second-order cone, making the relaxed problem a **second-order cone program (SOCP)**. SOCPs are convex and can be solved to global optimality in polynomial time using interior-point methods [13].

C. Exactness of the Relaxation

The relaxation (26) enlarges the feasible set relative to the original equality constraint. A critical question is whether the relaxation is *exact*—i.e., whether the optimal solution of the SOCP satisfies (18) as an equality.

Sufficient conditions for exactness [7], [8]:

1) The network graph $\mathcal{G}$ is a tree (radial topology).
2) The objective function is non-decreasing in l_{ij} (i.e., it penalises higher currents).
3) Voltage upper bounds are not binding.

For radial networks with loss-minimising objectives, the relaxation is generically exact. For meshed networks (such as our clustered-ring TC3), exactness is not guaranteed a priori but can be verified post-solve by checking the *SOCP gap*:

$$\Delta_{ij}(t) := v_i(t) \cdot l_{ij}(t) - P_{ij}(t)^2 \quad \forall (i,j) \in \mathcal{E} \tag{28}$$

If $\max_{(i,j),t} |\Delta_{ij}(t)| < \epsilon$ for a small tolerance ϵ (e.g., 10^{-4}), the relaxation is deemed exact and the SOCP solution is globally optimal for the original non-convex problem.

D. Convexity of the Converter Loss Model

The converter loss constraint (24) is a *convex* inequality for $\gamma > 0$, as $\alpha + \beta P_o + \gamma P_o^2$ is a convex quadratic. Combined with the epigraph formulation (minimising P_{conv_i} subject to $P_{\text{conv}_i} \ge f(P_{o_i})$), this preserves the SOCP structure.

The absolute value in (25) is handled via two linear inequalities:

$$P_{o_i}(t) \ge P^{\text{inj}}_i(t), \quad P_{o_i}(t) \ge -P^{\text{inj}}_i(t) \tag{29}$$

E. Computational Complexity

The resulting SOCP has $O(NT + ET)$ variables and $O(NT + ET)$ constraints, where $N = |\mathcal{N}|$, $E = |\mathcal{E}|$, and $T = |\mathcal{T}|$. Interior-point methods solve SOCPs in $O(n^{3.5})$ time, making the approach tractable for moderate-scale rural systems. For our largest test case (TC3: $N = 20$, $E = 24$, $T = 24$), the problem has approximately 6,700 variables and 12,000 constraints, solvable in under 20 seconds on a standard laptop.

VI. Test Systems and Data

Three test cases of increasing complexity are defined. All values are in per-unit on a 48 V, 1 kW base.

A. TC1: 7-Bus Radial System

A single cluster of 6 prosumer nanogrids plus one community load bus, connected in a radial topology:

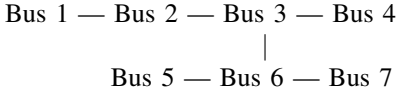

Bus 1 is the community load (school/clinic, no PV, no battery). Buses 2–7 are prosumer nanogrids with PV capacity 0.45–0.55 p.u., load demand 0.08–0.12 p.u., and battery capacity 2.0 p.u.-h. Line resistance: 0.04–0.06 p.u.

B. TC2: Modified IEEE 14-Bus DC System

Adapted from the IEEE 14-bus benchmark [5]: 13 prosumer nanogrids and one community load (Bus 14). Branch data is derived from the IEEE 14-bus system with reactance zeroed and resistance reduced by 10%. Zero-resistance branches (representing transformers in the AC original) are replaced with a small resistance (0.005 p.u.) to model DC-DC interconnecting links.

C. TC3: 20-Bus Clustered-Ring System

A novel topology designed to represent a practical village layout: 4 clusters of 4–5 nanogrids each. Within each cluster, nodes are connected in a *ring* topology to provide multiple power-sharing paths and resilience to single-link failures. The 4 clusters are interconnected via gateway nodes forming a higher-level ring. Bus 20 is a community load connected to the gateway of Cluster 1. Intra-cluster resistance: 0.04–0.05 p.u.; inter-cluster resistance: 0.06–0.07 p.u.

D. PV and Load Profiles

Time-varying profiles over a 24-hour horizon with hourly resolution are used:

- **PV generation**: Bell-shaped curve centred at solar noon (hour 12), with non-zero generation from hours 6–18. Based on typical tropical irradiance data from the National Renewable Energy Laboratory (NREL) [16].
- **Load demand**: Dual-peaked residential profile with a morning peak (hour 8) and a larger evening peak (hour 19), with overnight minimum. Based on rural load survey data [2].

Peak PV and load values per bus are scaled by these normalised multipliers at each hour.

E. Converter Parameters

The quadratic loss model $P_c = \alpha + \beta P_o + \gamma P_o^2$ uses coefficients $\alpha = 0.001$ p.u., $\beta = 0.02$, $\gamma = 0.03$, representative of modern high-efficiency DC-DC converters.

F. Solver

All problems are solved using CVXPY [14] with the CLARABEL interior-point solver [15]. Solver tolerance: 10^{-8}.

VII. Results

A. SOCP Exactness Verification

Table I reports the maximum SOCP gap $\max |\Delta_{ij}(t)|$ across all branches and time steps for each test case. In all cases, the gap is below 10^{-7}, confirming that the SOCP relaxation is exact and the solutions are globally optimal for the original non-convex problem.

TABLE I
SOCP Relaxation Exactness Verification

Test Case	Topology	Max SOCP Gap	Exact?
TC1 (7-bus)	Radial	1.45×10^{-8}	✓
TC2 (14-bus)	Meshed	2.17×10^{-8}	✓
TC3 (20-bus)	Clustered ring	2.30×10^{-8}	✓

TABLE II
24-Hour Cumulative Losses (p.u.) — OPF-1 vs. OPF-2

	OPF-1		OPF-2		
TC	Dist.	Total	Dist.	Conv.	Total
TC1	0.0320	0.0320	0.0358	0.3299	0.3656
TC2	0.0166	0.0166	0.0195	0.5262	0.5456
TC3	0.0568	0.0568	0.0643	0.7696	0.8339

B. Loss Comparison: OPF-1 vs. OPF-2

Table II summarises the 24-hour cumulative losses for both formulations across all test cases.

Key observation: OPF-1 reports only distribution losses (0.02–0.06 p.u. over 24 h), completely ignoring converter losses. When converter losses are properly accounted for in OPF-2, the *true* total system losses are an order of magnitude higher. This demonstrates that OPF-1 provides a fundamentally incomplete picture of system efficiency.

C. Hourly Loss Profiles

Fig. 1 shows the hourly total losses for TC3. OPF-2 losses follow the load profile shape, peaking during morning and evening demand periods when more power must be processed through converters. Distribution losses (visible in OPF-1) are comparatively small, confirming that converter losses dominate in typical rural DC microgrids with short distribution distances.

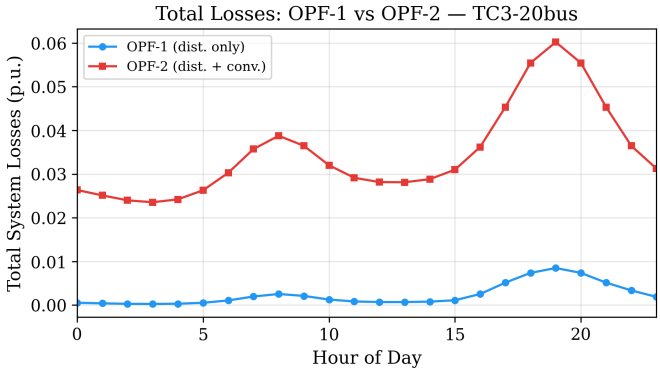

Fig. 1. Total system losses over 24 hours — TC3 (20-bus clustered ring).

D. Battery SOC Trajectories

Fig. 2 shows the battery SOC trajectories for TC1. Both formulations exhibit the expected pattern: batteries discharge overnight to serve loads, reach minimum SOC before sunrise,

charge during solar hours, and discharge again during the evening peak. The SOC limits (50%–90%) are respected throughout. OPF-2 produces slightly different dispatch patterns due to the additional converter loss awareness.

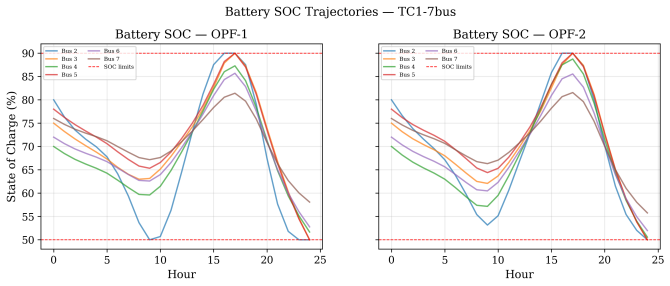

Fig. 2. Battery SOC trajectories over 24 hours — TC1 (7-bus radial).

E. Active Converter Count

Fig. 3 shows the number of active converters ($|P_i^{\text{inj}}| > 0.01\,\text{p.u.}$) per hour for TC2. During nighttime hours with battery-only operation, both formulations use 3–4 converters. During high-demand periods (hours 17–22), OPF-2 activates more converters but distributes power more evenly, whereas OPF-1 tends to concentrate flows.

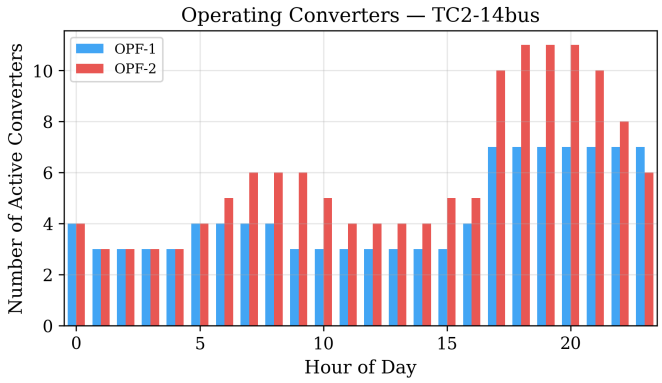

Fig. 3. Number of operating converters — TC2 (14-bus).

F. Voltage Profiles

Bus voltages remain within the $\pm 5\%$ limits across all test cases and time steps. Maximum voltage deviation occurs at buses furthest from the main power-sharing paths during peak load hours.

VIII. Discussion

A. Significance of Converter Loss Modelling

The results demonstrate a striking finding: **converter losses dominate distribution losses** in typical rural DC microgrids. For TC3, converter losses are approximately $12\times$ larger than distribution losses. This occurs because rural microgrids have short distribution distances (low resistance), but every unit of shared power must pass through at least one DC-DC converter with 5–15% losses. Studies that ignore converter losses (OPF-1) therefore underestimate total system losses by an order of magnitude.

B. Impact on Dispatch Decisions

OPF-2 produces qualitatively different dispatch decisions compared to OPF-1:

- **Power concentration vs. distribution**: OPF-2 is aware that activating a converter incurs a fixed cost (α), incentivising the system to process power through fewer, more highly loaded converters operating at higher efficiency. This effect is visible in the dispatch patterns.
- **Battery utilisation**: OPF-2 tends to keep batteries at higher SOC for longer, as discharging requires power to flow through converters.

C. SOCP Exactness

The SOCP relaxation was exact ($\Delta < 10^{-7}$) across all three test cases, including the meshed TC3 topology. This is an encouraging result, as exactness for meshed networks is not theoretically guaranteed. The exactness likely holds because the loss-minimising objective naturally discourages the relaxation from being slack.

D. Scalability

Solve times range from 5 s (TC1) to 18 s (TC3) for the full 24-hour problem on standard hardware. The SOCP structure enables polynomial-time solution via interior-point methods, making the approach viable for real-time dispatch in systems up to $\sim$100 buses. For larger systems, decomposition methods (e.g., ADMM) could exploit the clustered structure.

E. Limitations

1) **Centralised assumption**: The formulation requires full system observability and centralised computation. Distributed implementations (e.g., via ADMM) would be more practical but are not addressed here.
2) **Deterministic profiles**: Load and PV profiles are deterministic. Stochastic or robust extensions would be needed for practical deployment under forecast uncertainty.
3) **Ideal battery model**: Unity Coulombic efficiency and no degradation modelling limit the accuracy of long-term battery dispatch.
4) **No grid connection**: The current formulation is islanded only. Grid-connected operation with import/export pricing is left as future work, though the framework extends naturally by adding a slack bus at the point of common coupling (PCC).
5) **Converter model fidelity**: The quadratic polynomial is a simplified approximation. Piecewise-linear models could improve accuracy at the cost of additional binary variables (MISOCP).
6) **Synthetic test data**: While profiles are based on NREL data, the bus and branch parameters are synthetic. Validation against real field data from deployed rural microgrids would strengthen the results.

IX. Conclusion

This paper presented a loss-aware optimal power flow framework for DC community microgrids targeting rural electrification. By formulating the OPF as a second-order cone program via relaxation of the branch flow model, global optimality is achieved in polynomial time and verified post-solve. The key finding is that converter losses, which are entirely neglected in standard distribution-loss-only formulations (OPF-1), dominate total system losses in rural DC microgrids by an order of magnitude. This has significant implications for microgrid planning, sizing, and real-time dispatch: any framework that ignores converter losses will systematically overestimate system efficiency.

The framework was validated across three test cases—a 7-bus radial system, a 14-bus IEEE-derived system, and a novel 20-bus clustered-ring topology—with SOCP exactness confirmed in all cases. Future work will extend the formulation to grid-connected operation, incorporate stochastic profiles, and develop distributed solution algorithms suitable for deployment on low-cost embedded controllers.

References

[1] International Energy Agency, "SDG7: Data and Projections," IEA, Paris, 2023. [Online]. Available: https://www.iea.org/reports/sdg7-data-and-projections

[2] P. A. Madduri, J. Poon, J. Rosa, M. Podolsky, E. A. Brewer, and S. R. Sanders, "Scalable DC microgrids for rural electrification in emerging regions," *IEEE J. Emerg. Sel. Topics Power Electron.*, vol. 4, no. 4, pp. 1195–1205, Dec. 2016.

[3] M. Nasir, S. Iqbal, H. A. Khan, J. C. Vasquez, and J. M. Guerrero, "Sustainable rural electrification through solar PV DC microgrids—An architecture-based assessment," *IEEE Trans. Sustain. Energy*, vol. 11, no. 4, pp. 2017–2027, Nov. 2020.

[4] L. Richard, D. Frey, M.-C. Alvarez-Herault, and B. Raison, "A decentralized and communication-free control algorithm of DC microgrids for the electrification of rural Africa," *Sustain. Energy Grids Netw.*, vol. 32, 2022.

[5] R. Khan, M. Nasir, and N. N. Schulz, "An optimal neighborhood energy sharing scheme applied to islanded DC microgrids for cooperative rural electrification," *IEEE Access*, vol. 11, pp. 116956–116967, Oct. 2023.

[6] R. Khan, L. A. Akande, and N. N. Schulz, "Optimal neighborhood level power sharing in DC islanded microgrids for rural electrification," in *Proc. IEEE PES General Meeting*, 2024.

[7] L. Gan and S. H. Low, "Optimal power flow in direct current networks," *IEEE Trans. Power Syst.*, vol. 29, no. 6, pp. 2892–2904, Nov. 2014.

[8] Q. Li, R. Liu, Z. Wang, S. H. Low, and S. Mei, "Optimal power flow in stand-alone DC microgrids," *IEEE Trans. Power Syst.*, vol. 33, no. 5, pp. 5496–5506, Sep. 2018.

[9] D. Bienstock and A. Verma, "Strong NP-hardness of AC power flows feasibility," *Oper. Res. Lett.*, vol. 47, no. 6, pp. 494–501, 2019.

[10] B. Modu, M. P. Abdullah, M. A. Sanusi, and M. F. Hamza, "DC-based microgrid: Topologies, control schemes, and implementations," *Alexandria Eng. J.*, vol. 70, pp. 61–92, Mar. 2023.

[11] J. W. Kolar, F. Krismer, Y. Lobsiger, J. Muhlethaler, T. Nussbaumer, and J. Minibock, "Extreme efficiency power electronics," in *Proc. 7th Int. Conf. Integr. Power Electron. Syst. (CIPS)*, 2012, pp. 1–22.

[12] H. E. Gelani, F. Dastgeer, M. Nasir, S. Khan, and J. M. Guerrero, "AC vs. DC distribution efficiency: Are we on the right path?" *Energies*, vol. 14, no. 13, p. 4039, 2021.

[13] S. Boyd and L. Vandenberghe, *Convex Optimization*. Cambridge, U.K.: Cambridge Univ. Press, 2004.

[14] S. Diamond and S. Boyd, "CVXPY: A Python-embedded modeling language for convex optimization," *J. Mach. Learn. Res.*, vol. 17, no. 83, pp. 1–5, 2016.

[15] P. J. Goulart and Y. Chen, "CLARABEL: An interior-point solver for conic programs with quadratic objectives," 2024. [Online]. Available: https://github.com/oxfordcontrol/Clarabel.jl

[16] National Renewable Energy Laboratory, "National Solar Radiation Database (NSRDB)," NREL, Golden, CO. [Online]. Available: https://nsrdb.nrel.gov/